THE UNIVERSITY of EDINBURGH

Edinburgh Research Explorer

# Electrospun nanofiber substrates that enhance polar solvent separation from organic compounds in thinfilm composites

**Citation for published version:**
Lu, T-D, Chen, B-Z, Wang, J, Jia, T-Z, Cao, X-L, Wang, Y, Xing, W, Lau, CH & Sun, S 2018, 'Electrospun nanofiber substrates that enhance polar solvent separation from organic compounds in thinfilm composites', Journal of materials chemistry a, vol. 6, no. 31. https://doi.org/10.1039/C8TA04504F

**Digital Object Identifier (DOI):**
10.1039/C8TA04504F

**Link:**
Link to publication record in Edinburgh Research Explorer

**Document Version:**
Peer reviewed version

**Published In:**
Journal of materials chemistry a

**General rights**
Copyright for the publications made accessible via the Edinburgh Research Explorer is retained by the author(s) and / or other copyright owners and it is a condition of accessing these publications that users recognise and abide by the legal requirements associated with these rights.

**Take down policy**
The University of Edinburgh has made every reasonable effort to ensure that Edinburgh Research Explorer content complies with UK legislation. If you believe that the public display of this file breaches copyright please contact openaccess@ed.ac.uk providing details, and we will remove access to the work immediately and investigate your claim.

OPEN ACCESS

Download date: 12. Sep. 2019

Journal of Materials Chemistry A

# Electrospun nanofiber substrates that enhance polar solvent separation from organic compounds in thin-film composites



| | |
|---|---|
| Journal: | *Journal of Materials Chemistry A* |
| Manuscript ID | TA-ART-05-2018-004504.R1 |
| Article Type: | Paper |
| Date Submitted by the Author: | 25-Jun-2018 |





| | |
|---|---|
| Complete List of Authors: | Lu, Tian-Dan; Nanjing Tech University, State Key Laboratory of Materials-Oriented Chemical Engineering<br>Chen, Bo-Zhi; Nanjing Tech University, State Key Laboratory of Materials-Oriented Chemical Engineering<br>Wang, Jue; Nanjing Tech University, State Key Laboratory of Materials-Oriented Chemical Engineering<br>Jia, Tian-Zhi; Nanjing Tech University, State Key Laboratory of Materials-Oriented Chemical Engineering<br>Cao, Xue-Li; Nanjing Tech University, State Key Laboratory of Materials-Oriented Chemical Engineering, College of Chemical Engineering<br>Wang, Yong; Nanjing Tech University, State Key Laboratory of Materials-Oriented Chemical Engineering, College of Chemical Engineering<br>Xing, Weihong; Nanjing Tech University, State Key Laboratory of Materials-Oriented Chemical Engineering, College of Chemical Engineering<br>Lau, Cher Hon; University of Edinburgh, Chemical Engineering<br>Sun, Shi-Peng; Nanjing Tech University, State Key Laboratory of Materials-Oriented Chemical Engineering |



SCHOLARONE™
Manuscripts

Journal of Materials Chemistry A

PAPER

Received 00th January 20xx,
Accepted 00th January 20xx
DOI: 10.1039/x0xx00000x

www.rsc.org/

# Electrospun nanofiber substrates that enhance polar solvent separation from organic compounds in thin-film composites

Tian-Dan Lu,[a,b,c] Bo-Zhi Chen,[a,b,c] Jue Wang,[a,b,c] Tian-Zhi Jia,[a,b,c] Xue-Li Cao,[a,b,c] Yong Wang,[a,b,c] Weihong Xing,[a,b,c] Cher Hon Lau,[d*] Shi-Peng Sun[a,b,c*]

Organic solvent nanofiltration (OSN) with thin film composite (TFC) membranes containing a thin selective layer on top of a porous substrate is key to lowering energy costs of high-speed chemical separations. Conventional TFC membranes were often built on phase inversion induced asymmetrical substrates, with high tortuosity that impede rapid solvent transport. Nanofiber as ultrapermeable substrate has enhanced water transport in forward osmosis, nanofiltration and other aqueous separations. However, problems of solvent stability in harsh operating conditions prevent their exploitation in non-aqueous molecular separations. Here we show that by combining a simple solution-phase cross-linking process and electrospinning, the instability of nanofibrous polyacrylonitrile (PAN), in industrially-important polar solvents can be overcome and harnessed to benefit the purification of polar solvents containing low molecular weight solutes. The low tortuosity of electrospun PAN nanofibrous substrates is key to uniform cross-linking, hence are more stable and mechanically stronger than cross-linked PAN asymmetrical substrates fabricated by the traditional approach of phase inversion. The low resistance offered by cross-linked nanofibrous substrates increased solvent permeation without sacrificing selectivity, for example, to 99.5 % rejection of negatively-charge Sudan 4 (MW:380 Da) dyes with a methanol permeance of 9.87 L $m^{-2}$ $h^{-1}$ $bar^{-1}$ and water permeance of 22.40 $Lm^{-2}$ $h^{-1}$ $bar^{-1}$. The enhanced stability of TFC membranes in polar aprotic solvents such as dimethylsulfoxide highlight their potential application for molecular separations in pharmaceutical and chemical industries.

## 1. Introduction

Polar solvents such as alcohols, dimethylformamide (DMF), dimethyl sulfoxide (DMSO) are important industrial solvents as a reaction medium or reactant for organic syntheses,[1] polymer fiber spinning,[2] production of active pharmaceutical ingredients,[3] and fine chemicals.[4] As sustainable processes and development have become increasingly critical business strategies, there is a significant shift towards using solvents with low environment impact, safety and health risks. Amongst all polar solvents, alcohols and DMSO have been identified as "preferred" and "usable" industrial solvents.[5] For example, DMSO has been deployed in the pharmaceutical industry as a solvent for nucleophilic substitution reactions to synthesize antibiotics.[6] Upon removal of the targeted product, catalysts and other by-products are present in the organic solvent effluent. Traditionally, such effluents are discharged or incinerated.

Alternatively, distillation can be a more sustainable process to recover and recycle organic solvents. However, the energy consumption of distillation processes can be very high as large amounts of heat are required to overcome high solvent boiling points or separate azeotropes. The deployment of heat-based processes can be highly dangerous.[7] Clearly, solvent recovery must be achieved with a green, and relatively mature technology to lower both solvent usage and carbon footprint of the pharmaceutical industry in a sustainable manner.

Organic solvent nanofiltration (OSN), a separation technology based on size-exclusion, can potentially reduce the energy consumption of organic solvent recovery.[8, 9] OSN membranes can exist as thin-film composites (TFC) where thin selective polymer layers are deposited on to porous substrates that are fabricated from different polymers. Polyamides that are stable in organic solvents are the preferred polymer choice for the selective layer of most TFC membranes.[10, 11] Meanwhile, porous substrates are typically fabricated from polysulfones, polyethersulfones, polyacrylonitrile (PAN) – polymers that are compatible with polyamides but are only stable in alcohols and not in aprotic solvents such as DMSO and DMF.[12] Hence, the solubility of porous substrates must be resolved to maximize the benefits of TFC membranes for OSN.

Cross-linking is often deployed to link the polymer chains to prevent polymer dissolution in solvents. For example, cross-linking stabilized the selective layers of TFC membranes fabricated from polybenzimidazole[13] and polyimide[14] in DMF whilst demonstrating enhanced separation performances at

[a] State Key Laboratory of Materials-Oriented Chemical Engineering
Email: ssp@njtech.edu.cn, ssp@live.com Tel:+86-25-83587560
Website:www.sun-membrane.com,
[b] Jiangsu National Synergetic Innovation Center for Advanced Materials
[c] College of Chemical Engineering, Nanjing Tech University, Nanjing 210009, China
[d] School of Engineering, University of Edinburgh, Robert Stevenson Road, Edinburgh EH9 3FB, UK. Email: cherhon.lau@ed.ac.uk

This journal is © The Royal Society of Chemistry 20xx



Please do not adjust margins

the expense of lower fluxes. Chen and co-workers cross-linked choromethylated polysulfone membranes to facilitate the separation of dyes from a range of polar solvents – aprotic (N,N-dimethylacetamide) and protic (alcohols).[15] Musale and Kumar cross-linked chitosan/PAN with glutaraldehyde to fabricate OSN membranes that were stable in alcohols, ketones, esters and aliphatic hydrocarbons at various pH levels.[16] However, polymer cross-linking slows down solvent transport as the mass transfer resistance increases with polymer densification (due to cross-linking) in both the selective layer and the porous substrate. [17]

A potential strategy to overcome the impact of polymer densification on solvent transport after cross-linking is to utilize porous substrates with low tortuosity and high concentrations of large pores. Substrates with large pores also encourage the formation of thinner selective layers that can also enhance solvent permeance;[18, 19] whilst minimizing the impact of polymer densification within the substrate.[20] Polymer substrates with large pores and superior mechanical stability can be fabricated with electrospinning[21, 22]– a simple approach to wet-spin polymer nanofibers from solutions using the electrostatic forces within an electrical field.[23] The inter-fiber pores are large (μm size), while the stacking of polymer nanofibers provide mechanical stability. Hence, electrospun nanofiber substrates are ideal for membrane separations. [24, 25] For example, electrospun PAN, polysulfone, polyvinylidene fluoride and poly(vinyl alcohol) nanofiber substrates were first harnessed to drastically enhance water permeability in TFC forward osmosis membranes.[26-30] These polymers were chosen for their compatibility with polyamide selective layers fabricated from interfacial polymerization of amines and acyl chlorides.[30, 31] The tortuosity and porosity of electrospun nanofiber substrates may enhance solvent transport, yielding highly permeable membranes. However, this also increases the exposure of polymers to solvents that may enhance polymer dissolution.

Here we propose to optimize polymer cross-linking impact *via* the low tortuosity of electrospun nanofiber substrates to stabilize acrylic polymer substrates for the recovery of polar solvents. As a proof of concept, here we have chosen a commercially available acrylic polymer – PAN to fabricate the porous substrate. PAN is easy to work with, have excellent adhesion properties, and superior mechanical properties.[32] However, PAN is not stable in aprotic solvents. Methods have been reported to enhance chemical stability of PAN membranes like copolymerization[33] and cross-linking[34] . Herein, hydrazine hydrate was used as the cross-linker for its simplicity, easy availability and low price to engineer a cross-linked PAN nanofibrous substrate of good stability in polar solvents. We also compared the impact of the physical configuration (nanofibrous substrates vs traditional asymmetrical substrates from phase inversion, **Fig. 1**) of PAN porous substrates on cross-linking, mechanical strength and consequently PAN stability in polar aprotic solvents. To demonstrate the potential application of stabilized PAN nanofiber substrates, a polyamide selective layer fabricated by interfacial polymerization was deposited on top of these nanofiber substrates. The resultant TFC membrane was stable in DMSO for up to 50 hours, whilst rejecting more than 95 % of 50 ppm dissolved dyes of different charges and sizes. The physical properties of these dyes were summarized in **Table. S1** (Supporting Information). The outcomes of this study can provide insightful guidelines for developing next-generation OSN membranes for rapid and stable molecular separations.

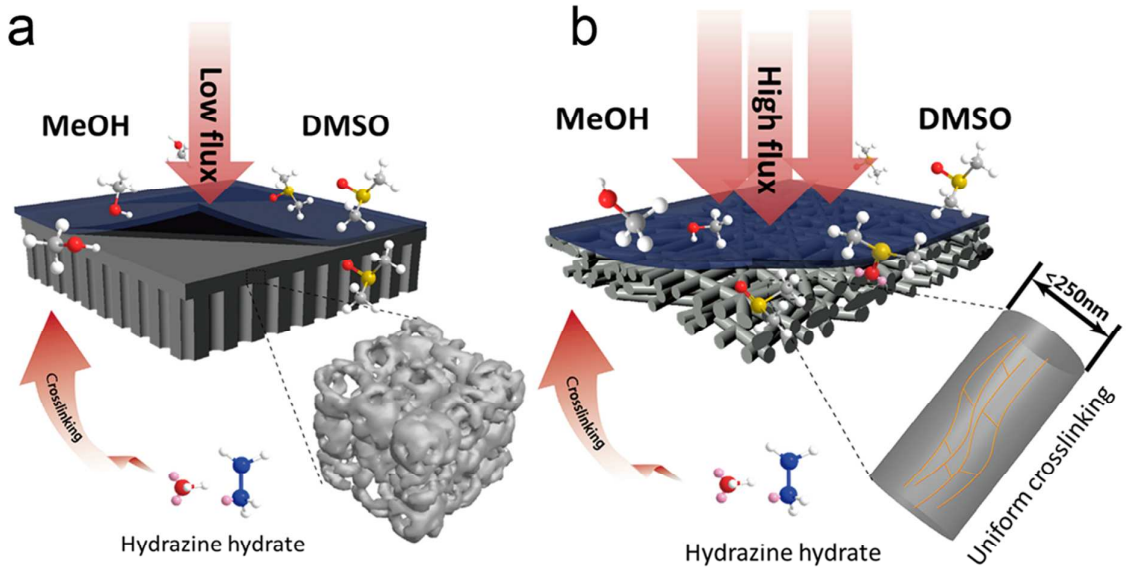


**Fig. 1** TFC membranes comprising (a) asymmetrical and (b) nanofibrous substrates produced from phase-inversion and electrospinning, respectively.



Please do not adjust margins

## 2. Experimental

### 2.1 Materials

Commercially available polyacrylonitrile (PAN, MW = 85, 000 Da) was used to prepare the substrates. N, N-dimethylformamide (DMF, AR), piperazine (PIP, >99.0 %), trimesoyl chloride (TMC, 98 %), n-hexane (>99.9 %), hydrazine hydrate (HH, 50 %) were purchased from Aladdin. PIP, TMC, n-hexane were deployed for polyamide interfacial polymerization, while HH was used to cross-link PAN. PEG 100, PEG 200, PEG 400 and PEG 1000 were purchased from Merck to characterize the molecular weight cut-off (MWCO) of the membrane. Methanol (99.99 %, AR), dimethyl sulfoxide (DMSO, AR), N, N-dimethylformamide (DMF, AR) purchased from Aladdin were used as solvents for permeation tests. Sudan IV (380.44 g $mol^{-1}$), Crystal Violet (407.98 g $mol^{-1}$), Fast Green FCF (808.91 g $mol^{-1}$) and Reactive Black (991.82 g $mol^{-1}$) were purchased from Aladdin for NF studies. The molecular structures of these dyes are listed in **Table S1**.

### 2.2 TFC fabrication

PAN powder was dissolved in DMF, and stirred at 60 °C for 6 hours to obtain a 10 wt.% homogenous solution. A 20 mL as-prepared spinning solution was electrospun on to aluminium foil under an electrical field with optimized voltage (20 kV), flow rate (1.0 mL $h^{-1}$) and distance between the needle tip and the collector (14 cm). The nascent nanofiber mat was peeled off from the aluminium foil and placed into an oven at 80 ºC for 12 hours to ensure complete removal of remainder solvent trapped with the nanofibers. Electrospun PAN nanofibrous mats were hot-pressed at 95 ºC at 0.25 MPa for 40 min to improve mechanical strength whilst obtaining a smooth surface for the subsequent deposition of PA selective layers.

For comparison, homemade asymmetrical PAN substrates were produced by casting a 12 wt% PAN/DMF polymer solution on to a glass plate with a 200 µm thick casting knife at a casting speed of 0.025 $ms^{-1}$. Asymmetrical PAN substrates were immersed in a water coagulant bath (room temperature) for phase separation. Both PAN nanofibrous and asymmetrical substrates were cross-linked at 85°C in an aqueous solution containing 20 % (v/v) of hydrazine hydrate and deionized water at various durations.

Thin polyamide (PA) selective layers were deposited on to PAN substrates *via* interfacial polymerization between PIP and TMC. The surfaces of both the nanofibrous and asymmetrical substrates were first exposed to an aqueous basic solution of PIP (1 % w/v) for 2 min. Excessive PIP was first removed from PIP-loaded substrates using a rubber roller prior exposure to hexane solutions containing 0.1 % w/v TMC for 2 min. Unreacted reagents were removed from the thin-film composites by filtration with pure DMF in a dead-end permeation cell at 10 bar for 10 min. The resulting TFCs were washed with DI water for several times and finally stored in DI water at room temperature before characterization. The fabrication process of TFC membranes studied here in this work is shown in **Fig. S1** (Supporting information).

### 2.3 TFC characterization

TFC morphologies were observed from freeze-dried samples with a scanning electron microscope (SEM, Hitachi S4800). To obtain a clean edge for cross-sectional imaging, the membranes were first frozen in liquid nitrogen, cracked, and sputter-coated with a thin layer of gold before imaging. An accelerating voltage of 5 kV was used to obtain SEM micrographs. The diameter distribution of fibers was determined from 30 random fibers.

ATR-FTIR was used to confirm the cross-linking mechanism and the cross-linking degree of PAN substrates. An attenuated total reflectance (ATR) mode was applied using a Fourier transform spectrometer (FT-IR, Thermo Scientific, Nicolet iS50) over the range of 600–4000 $nm^{-1}$ with 64 scans for each sample. The samples were dried for 12 h in a vacuum oven before analysis.

X-ray photoelectron spectroscopy (XPS) depth profiling was used to reveal the type of nitrogen-containing groups in the substrates. The measurements were carried out on a XPS system (Thermo Fisher K-Alpha, USA) equipped with a hemispherical electron analyser operating with a focusing lens at variable spot sizes from 100 to 800 µm and at a typical take-off angle of 45º. The ion gun utilized for sputtering is equipped with a special gas-flow regulating system, which enabled automated operation even during lengthy depth profiling experiments. Polymers were removed by etching with $Ar^+$ ions with energy of 3.5 keV, intensity of 1.0 µA, the ion beam scanning area is 3 mm × 3 mm, the sputtering rate was set to 3 nm/min.

X-ray diffraction (XRD) patterns of PA/PAN TFCs studied here were collected at 2θ = 2.5° to 30° with a 2θ step of 0.02° using CuKα radiation on a RigakuSmartlab equipment.

The gel content of cross-linked PAN substrates was determined by extracting the samples in aprotic solvents for 24 h. Insoluble fractions were washed with DI water and vacuum-dried at 80 °C for 24 h prior weighing. Gel content reduction ratio was calculated from the mass of cross-linked PAN films using the following equation:

$$\text{Gel Content Reduction\%} = \left(1 - \frac{W_1}{W_0}\right) \times 100\% \quad (1)$$

where $W_1$ and $W_0$ masses of the cross-linked PAN samples prior and after solvent extraction, respectively.

The surface area and pore volume of PAN nanofibers studied here in this work were characterized by nitrogen adsorption-desorption tests (Micromeritics, TriStar II Plus) and calculated using Brunauer-Emmett-Teller (BET) and Barrett-Joyner-Halenda (BJH) methods. All the samples were transferred to pre-dried analysis tubes, sealed with Transeal stoppers, evacuated, and activated at 90 ºC under a $10^{-6}$ dynamic vacuum for 14 h. Ultrahigh purity $N_2$ gases were used for these experiments. $N_2$ adsorption measurements were conducted at 77 K.

The surface charges of TFCs studied here were analyzed using a SurPASS electrokinetic analyzer (AntonPaar GmbH, Austria) through streaming potential measurements. A 0.1 M



Please do not adjust margins

KCl solution was circulated through the measuring cell containing the membrane sample. Automatic titrations with 0.1 M HCl and 0.1 M NaOH were carried out to study the pH dependence of the zeta potential and thus determine the isoelectric point with the method described previously. [19]

The total porosity of the substrate samples was determined by filling the pores of a pre-weighed substrate sample using kerosene with density 0.8 g $mL^{-1}$. Kerosene-loaded samples were weighed and the volume of pore-filling liquid was obtained by the following equation:

$$\text{Porosity}=\frac{W_w - W_d}{A \cdot d \cdot \rho} \quad (2)$$

where A is the surface area of the sample ($m^2\ g^{-1}$) , d is the average thickness of the substrate (μm), ρ is the kerosene density (g $cm^{-3}$ ) and $W_w$ , $W_d$ are the mass of the wetted and dry samples (g), respectively.

The average pore size of the substrate samples was determined by means of mercury porosimetry (AutoPore IV 9500, Micromeritics').

The mechanical properties of the PAN substrates were measured at room temperature using a tensile testing machine (CMT-6203, Shenzhen Xinsansi). The substrates were cut into 5 mm × 7 cm strips, and the thickness of specimen was in the range of 150-200 μm. The stretching speed was 10 mm $min^{-1}$.

The effect of cross-linking on the hydrophilicity of PAN substrates was analysed with a static contact angle water-membrane measurements in a contact angle measuring instrument (Drop Meter A100P) with 2 μL volume drops. Samples were freeze-dried before characterization.

**2.4 Separation performances of TFCs**

Membrane separation performance parameters including pure water permeability (PWP) and rejection were characterized using a dead-end filtration system. Prior membrane characterization, each sample was flushed with deionized water for more than 60 minutes to ensure that the film reached steady state. Highly pressurized DI water (with nitrogen) was deployed here to determine the PWP (L $m^{-2}$ $bar^{-1}$ $h^{-1}$) of each membrane. PWP was calculated with the following equation:

$$\text{Permeance} = \frac{Q}{\Delta P \cdot A_m} \quad (3)$$

where Q is the water permeation volumetric flow rate (L $h^{-1}$), $A_m$ is the effective filtration area ($m^2$), and ΔP is the trans-membrane pressure (bar).

The TFCs were characterized by solute separation experiments with four 50 ppm dye solutions. The solute rejection $R_t$ (%) was calculated using the following equation:

$$R_t(\%) = 1 - \frac{c_p}{c_f} \quad (4)$$

where $c_p$ and $c_f$ are the solute concentrations in the permeate and the feed solution, respectively. The concentrations of the dye solutions were tested with a UV spectrometer (UV2450, Shimadzu) over the range of 400–700 $nm^{-1}$ for the absorbance spectra and calculated with absorption peak value at wavelengths of 514.0, 617.5, 615.0, and 598.5 $nm^{-1}$ for Sudan IV, Crystal Violet, Fast Green FCF and Reactive Black, respectively.

The MWCOs of membranes were estimated by various neutral organic solutes. Similar to the performance testing process, mixed solutions comprising PEGs with different molecular weights (PEG 100, PEG 200, PEG 400 and PEG 1000, each of a 1% w/v concentration) were pressed through the TFC membrane at 4 bar. The solutions before and after filtration were tested by gel permeation chromatography (GPC,1515, Waters, USA) and formula (4) was used to calculate the rejection R (%).

## 3. Results and Discussions

**3.1 Fabrication of PAN substrates**

Porous PAN substrates with different tortuosity factors were fabricated using phase inversion and electrospinning techniques. PAN substrates produced from phase inversion were asymmetrical where a dense skin layer was observed on top of irregular-shaped macro-voids (**Fig.2a**), while pristine PAN nanofiber substrates comprised overlapping nanofibers with average diameters of 210 nm (**Fig. 2c**). After hot pressing for 40 mins at 0.25 MPa and 95 ºC, the diameters of PAN nanofibers were increased to 246 nm (**Fig. 2b**). Hot-pressing ensured close contact between each PAN nanofiber whilst preventing compression at higher pressures.[35] Cross-linking hot-pressed nanofiber substrates with hydrazine hydrate increased the average nanofiber diameter to 255 nm (**Fig. 2d**).

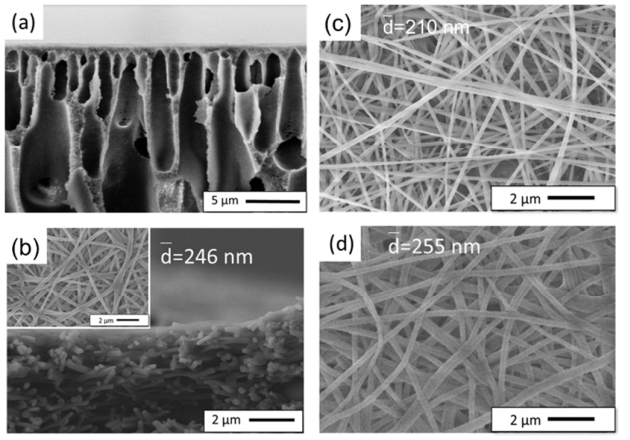


**Fig.2** SEM micrographs shows the cross-section of (a) asymmetrical and (b) nanofibrous PAN substrates(The inset figure shows the surface of hot-pressed PAN nanofiber substrates). The average nanofiber diameter in pristine nanofiber mats increased from 210 nm to (c) 246 nm after hot-pressing and(d) 255 nm after cross-linking.

As shown in Table 1, the pure water permeance of nanofibrous substrates is 13.6 times higher than asymmetrical substrates, which may result from the relatively low tortuosity. The thickness and porosity of the two substrates were kept similar.

To obtain the tortuosity, the performance parameters can be calculated based on Hagen–Poiseuille model, commonly used for aqueous systems permeating through porous media36:

Table 1. Summary of PAN substrate characteristics

| Type of PAN substrate | Average thickness (μm) | Porosity (%) | Average pore diameter(nm) | Tortuosity | Pure water permeance ($Lm^{-2}h^{-1}bar^{-1}$) |
|---|---|---|---|---|---|
| **Asymmetric** | 185.5±15 | 59.8±1 | 333.5 | 6.86 | 585.9±50 |
| **Nanofibrous** | 200.0±15 | 65.9±1 | 603.2 | 1.62 | 7950.0±50 |

$$J = \frac{B}{\eta}\Delta P \quad (5)$$

Where η is the pure water viscosity (1.004 mPa•s) and B the substrate permeability which is defined as:

$$a = \frac{\varepsilon r^2}{8\tau\Delta\delta}\Delta P \quad (6)$$

Where r is the (hydrodynamic) pore radius, Δδ is the layer thickness, ε is the porosity, and τ is the tortuosity.

The tortuosity τ of the substrates can be calculated using Equation (7):

$$\tau = \frac{8J\eta\Delta\delta}{\varepsilon r^2 \Delta P} \quad (7)$$

The performance and structure parameters of different substrates are concluded in Table 1. It can be concluded that the nanofibrous substrate possesses significantly lower tortuosity which offers low solvent transport resistance. [26] Moreover, it also provides more efficient crosslinking, as described in the following section.

### 3.2 Impact of substrate structure on PAN cross-linking

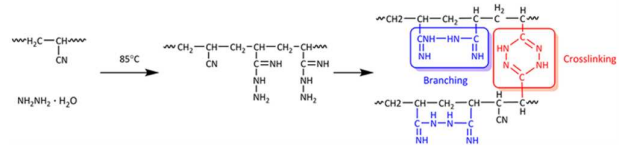


**Scheme 1** Proposed mechanism underpinning PAN cross-linking using hydrazine hydrate.

Hydrazine hydrate cross-linking is a well-established protocol to stabilize PAN in polar aprotic solvents such as DMSO and DMF.[34, 37] Using this protocol, we investigated the impact of substrate structure on the degree of PAN cross-linking and organ stability. FTIR (Fig. 3a) was used here to track the cross-linking reaction between hydrazine and the PAN C≡N functional groups over 24 hours. As cross-linking duration increased from 0 to 24 hours, the intensity of the peak corresponding to C≡N functional groups centred at 2243 cm-1 diminished. The new broad absorption peak in the 1665-1630 $cm^{-1}$ region is for the stretching vibrations of C=N and N-N bands and the 1200 -1310 $cm^{-1}$ peaks are assigned to the mixed C-N stretching and N-H bending vibrations, which are broadened due to the conjugation effect, confirming the predominant formation of cyclic nitrogen-containing structures.[34, 38, 39] This indicated the transformation of linear C≡N functional groups into cyclic, nitrogen-containing structures (cross-linking) or hydrazides (branching) as shown in Scheme 1.[40]

**Table 2.** Nitrogen distribution on the polymer chain as a function of measure depth

| Type of Substrates | Approximate depth from surface (nm) | Ratio of functional group(%) Cyclization N-N (I) [a] | C=N-N | Acyclic N-N (II) | C=N |
|---|---|---|---|---|---|
| Asymmetric-8 | 0 | 88.13 | 0.12 | 0.16 | 9.69 |
| | 60 | 12.81 | 0 | 0.12 | 76.72 |
| | 120 | 3.26 | 0.02 | 9.05 | 62.60 |
| Nanofibrous-8 | 0 | 29.69 | 15.96 | 19.88 | 20.35 |
| | 60 | 27.85 | 6.36 | 27.85 | 26.55 |
| | 120 | 21.49 | 6.89 | 32.03 | 31.73 |

a) N-N (I) stand for nitrogen atoms in the cyclic structure, N-N (II) stand for nitrogen atoms in the alkane groups.

The cross-linking duration drastically impacted on the mechanical properties of PAN nanofibrous substrates (**Fig. 3b**). The tensile strength of nanofibrous substrates increased from 10 MPa to 16 MPa when hydrazine cross-linking duration increased from 0 to 8 hours. Beyond 8 hours of cross-linking, the tensile strength of nanofibrous substrates were reduced to 10 MPa. The reduction of tensile strength beyond optimal cross-linking duration was attributed to excessive polar functional groups and large substituents that impeded the segmental mobility of PAN polymer chains,[41] embrittling and deforming PAN nanofibers at lower strain levels.

Hydrazine cross-linking also impacted on the amorphous regions of PAN nanofibrous substrates (**Fig. 3c**). XRD spectra of PAN usually consist of two peaks centred at 2θ = 17˚ and 29˚, corresponding to *d*-spaces of 5.2 and 6.0 Å, respectively.[42] The 5.2 Å *d*-space arises from the (100) diffraction of a hexagonal lattice made up of closely-packed parallel molecular rods, while the 6.0 Å *d*-space corresponds to the (110) PAN crystallographic plane.[43] The broadening of the intense peak at 2θ= 17˚after 24 hours of hydrazine cross-linking indicated the retention of the original PAN crystal lattice even after branching and cross-linking. Meanwhile, the peak centred at 2θ=29˚ diminished after 8 hours of hydrazine cross-linking. This was due to the branching and linking of PAN amorphous regions that are intertwined between crystalline regions.[44] The branching and linking up of amorphous regions within PAN nanofibers increased intra-fiber porosity as the Bruaunuer Emmett Teller (BET) surface area of cross-linked fiber mats were enhanced by 16 %, from 8.01 $m^2 g^{-1}$ to 9.26 $m^2 g^{-1}$ (**Table S2**). With maximum mechanical strength, the optimal cross-linking duration to modify PAN nanofibrous substrates is 8 hours.

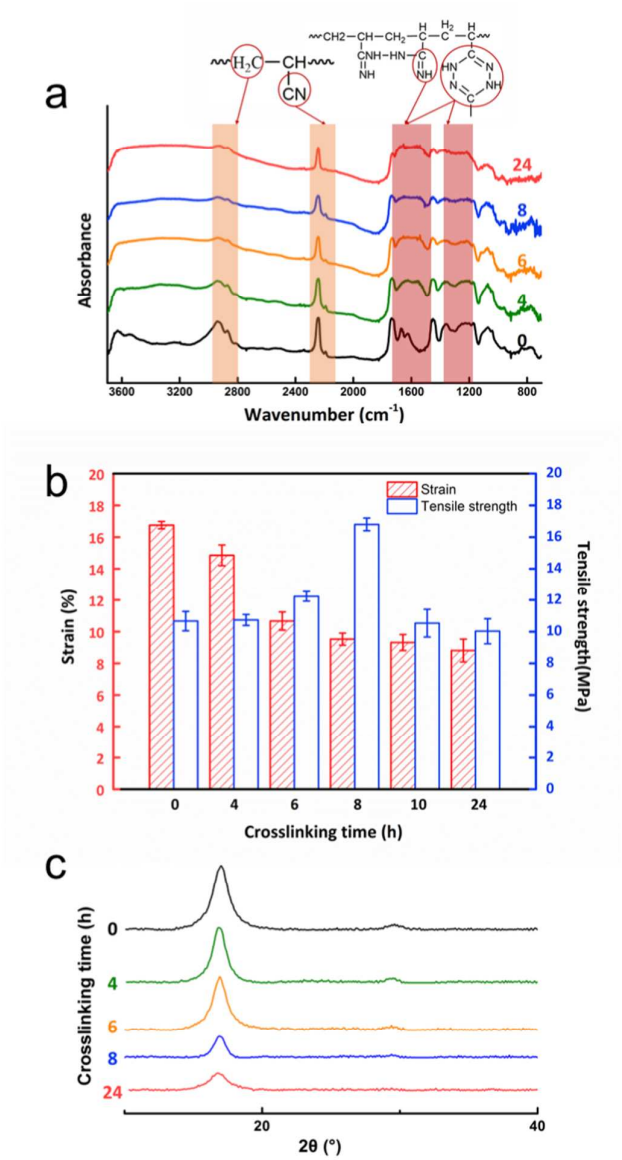


**Fig.3** The impact of cross-linking duration (0 h – black, 4 h – green, 6 h – orange, 8 h – blue and 24 h – red) on (a) chemical structure of PAN, (b) PAN mechanical properties, and (c) PAN crystallinity.

The impact of substrate tortuosity and porosity on cross-linking degree in various PAN substrates was determined from the distribution of nitrogen-containing functional groups obtained from XPS depth-profiling. Substrate surfaces were etched with an Ar-laser for 300 s. Each 30-second laser sputtering cycle removed 12 nm of polymeric material. The ratios of various N-based functional groups in both cross-linked asymmetrical and nanofibrous substrates for different depths beneath the surface are summarized in **Table 2**. The surface of cross-linked asymmetrical substrates comprised 88.13 % and 9.69% of cyclic and acyclic nitrogen-based functional groups, respectively. The concentration of cyclic nitrogen was drastically reduced to 12.81 and 3.26 %, at 60 and 120 nm into the bulk of cross-linked asymmetrical substrates, respectively.

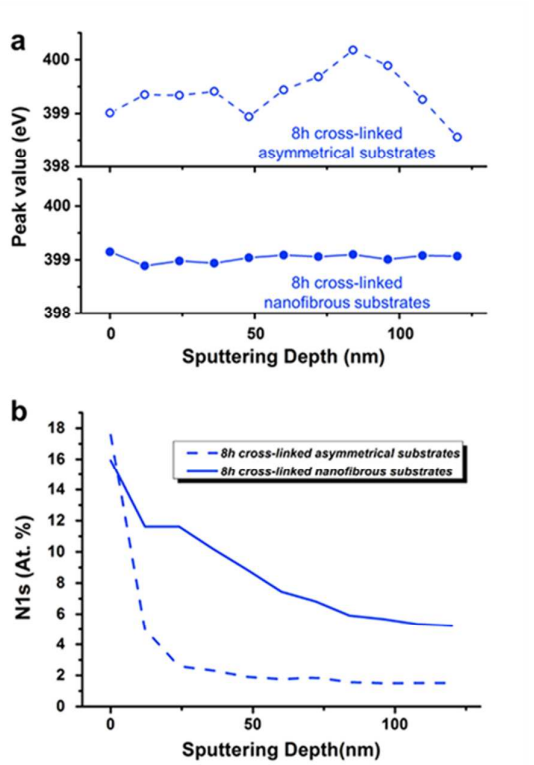


**Fig. 4** (a) Depth dependent N1s main peak value shift on the binding energy scale during XPS depth profiling of the argon ion laser treated samples (b) Depth dependent N content during XPS depth profiling of the argon ion laser treated samples.

The dense skin layer of these substrates could have impeded the penetration of hydrazine hydrate molecules, leading to non-uniform cross-linking that caused the uneven distribution of cyclic nitrogen functional groups. This drastic change in nitrogen-type is also observed in binding energy shift of the N 1s main peaks at different depths of the asymmetrical PAN substrate (**Fig. 4a**). The N 1s atomic concentration was reduced exponentially in a short etching time (**Fig. 4b**).

Meanwhile, the surface and bulk of cross-linked nanofibrous substrates contained identical amounts of cyclic N-based functional groups (**Fig. S2, Table 2, Fig. 4a**). The low tortuosity of nanofibrous substrates exposed a higher surface area of PAN to hydrazine cross-linking, leading to more uniform distribution of N 1s content on both the surface and up to 120 nm within the bulk (**Fig. 4b**).

A key advantage of solution hydrazine cross-linking is improving the stability of PAN nanofibrous substrates in organic solvents. This is ascribed to the higher conversion of C≡N functional groups in nanofibrous substrates that resulted in higher gel content after prolonged exposure to polar aprotic solvents such as DMSO and DMF (**Table S3**). Here it is important to point out that the Hansen solubility parameter of



Please do not adjust margins

PAN (27.4 $MPa^{1/2}$) is closer to that of DMSO (26.68 $MPa^{1/2}$) than DMF (24.86 $MPa^{1/2}$),[45] and the nucleophilicity of -S=O is higher than that of -N-CHO. Combined, these effects will lead to stronger solvation effects on electrophilic –C≡N chain segments by DMSO; resulting in lower gel content after immersion in DMSO. The solvent stability of both cross-linked substrates in DMF and DMSO are shown in **Fig. 5a**. The physical appearance of cross-linked nanofibrous substrates remained intact even after soaking in both aprotic solvents for 48 hours. Meanwhile, the colour of cross-linked asymmetrical substrates faded upon immersion in both DMF and DMSO. This was indicative of partial PAN dissolution in these solvents. This was ascribed to less uniform hydrazine cross-linking in asymmetrical substrates.[46, 47]

The higher conversion rate of C≡N functional groups in cross-linked nanofibrous substrates led to superior mechanical properties when compared to cross-linked asymmetrical substrates (**Fig. 5b** and **Fig. S3**).[48] This could be attributed to several factors. Firstly, the irregularly shaped macro-voids in asymmetrical substrates might bear inconsistent strain; lowering strain tolerance[22]. Second, the high electric field deployed during PAN electrospinning might orientate crystalline PAN domains,[49] forming substrates with high tensile strength, modulus and toughness. Third, non-homogeneous densification of PAN asymmetrical substrates during cross-linking could cause the surface and bulk to contract at different rates;[50] drastically lowering strain values **(Fig. 5c)**.

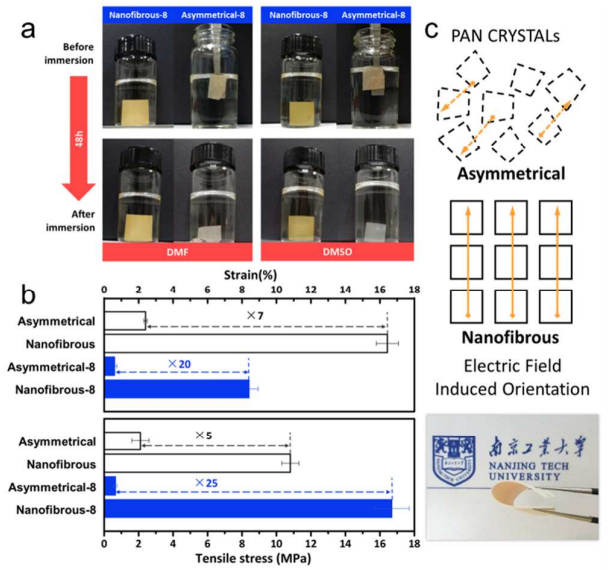


**Fig. 5** (a) Photographs of 8h-cross-linked nanofibrous and asymmetrical substrate appeareance before and after immersion in aprotic solvent, (b) Influence of cross-linking on mechanical strength, (c) the electric field induced orientation of PAN crystals in nanofibrous substrates comparing with disordered arrangement of which in asymmetrical substrates.

### 3.3 Organic solvent nanofiltration performances of TFCs

TFC membranes were fabricated here by depositing thin polyamide (PA) selective layers on the surfaces of various substrates using interfacial polymerization between piperazine and trimesoyl chloride. The selective PA layers deposited on the low tortuous nanofibrous substrates were slightly thinner than that on asymmetrical substrates that were less tortuous from the SEM image (**Fig. 6**). The large inter-fibre pores in nanofibrous substrates might account for formation of polyamide inside the pore and thinner skin layer.[51]

Membrane separation experiments were performed at 10 bar, 25 °C using a dead-end cell with constant stirring at 400 rpm. We characterized these TFCs using water, methanol and DMSO. The pure water permeance of TFC membranes comprising cross-linked nanofibrous substrates was 22.4 $Lm^{-2}h^{-1}bar^{-1}$–9 times higher than those observed with cross-linked asymmetrical substrates (**Fig. 6c**). The lower resistance against molecular transport of nanofiber substrates was key to drastically enhancing pure water permeance in TFCs fabricated with cross-linked nanofibrous substrates.

The cross-linking duration of cross-linked nanofibrous substrates drastically impacted on water transport. As shown in **Fig. 7a**, the water permeances of TFC membranes containing PAN nanofibrous substrates cross-linked for 4 hours were reduced by 50%. However, water transport was enhanced with longer periods of hydrazine cross-linking. This was because hydrazine cross-linking reduced both the water contact angle of PAN nanofibrous substrates from 75 ° to 32 ° (**Fig. 7b**), and the time required for the water contact angle to reduce. For example, a 42% reduction in water contact angle was achieved in 6 seconds in pristine PAN nanofibrous substrates. The water contact angle of PAN nanofibrous substrates that were cross-linked for 24 hours was reduced by 82 % in less than 2 seconds.

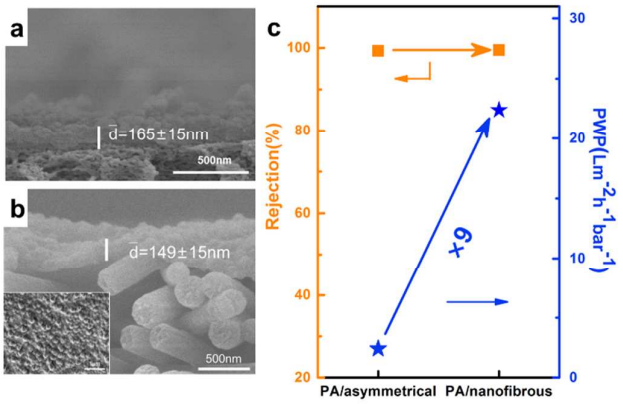


**Fig. 6** cross-sectional SEM image of (a)PA/asymmetrical PAN substrate and (b) PA/ nanofibrous PAN substrate; (c) comparison of PWP and rejection in FCF/water system between TFCs studied here.

The effects of fabrication conditions of TFC membranes comprising cross-linked nanofibrous substrates were studied using mixtures of methanol and four types of molecular dyes with different molecular weights and charges (**Table S1**). Cross-linking duration did not impact on the methanol permeance of TFC membranes comprising PAN nanofibrous substrates, but enhanced dye rejections. The absorbance spectra at wavelengths between 400 and 700 nm are shown in **Fig. S4**. The retention rates of negatively-charged dyes such as

Sudan IV, Fast Green FCF and Reactive Black were more than 99 %, while the rejection of positively-charge Crystal Violet was lower. This was due to the Donnan exclusion effect underpinning the separation mechanism of TFC membranes studied here.[52]

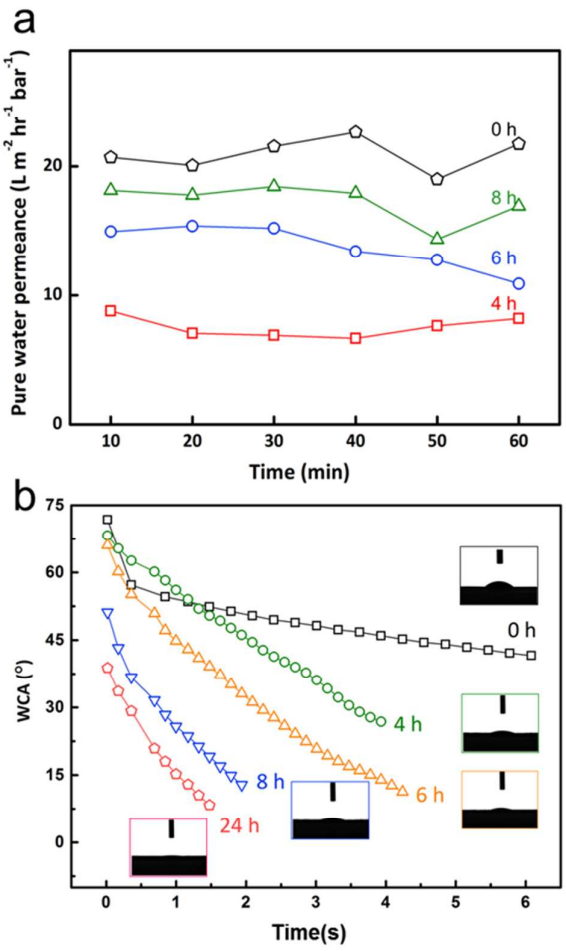


**Fig.7** (a)The pure water permeance of TFC membranes comprising PA/ cross-linked nanofibrous substrates with prolonged cross-linking time. (b) Time-dependent water contact angle of cross-linked nanofibrous substrates.

As the molecular weight of all dyes used here were above the MWCO of 300 Da (determined using polyethylene glycol of various sizes, **Fig. S5**), the rejection of the negatively-charge dyes was governed by repulsion from the PA surface that was negatively charged. The isoelectric point of TFC membranes containing cross-linked PAN nanofibrous substrates was at pH 4.2. The zeta potential curve of the polyamide surface (**Fig. S6**) was typical of an amphoteric surface where carboxyl and amine functional groups are present.[53] A positively-charge polyamide surface below pH 4.2 was due to the protonation of amine functional groups, while the deprotonation of carboxyl groups led to a negatively-charge polyamide surface above the isoelectric point at pH 4.2. The impact of carboxyl deprotonation outweighed the effect of amine protonation; indicative of a higher carboxyl content in the PA selective layer.

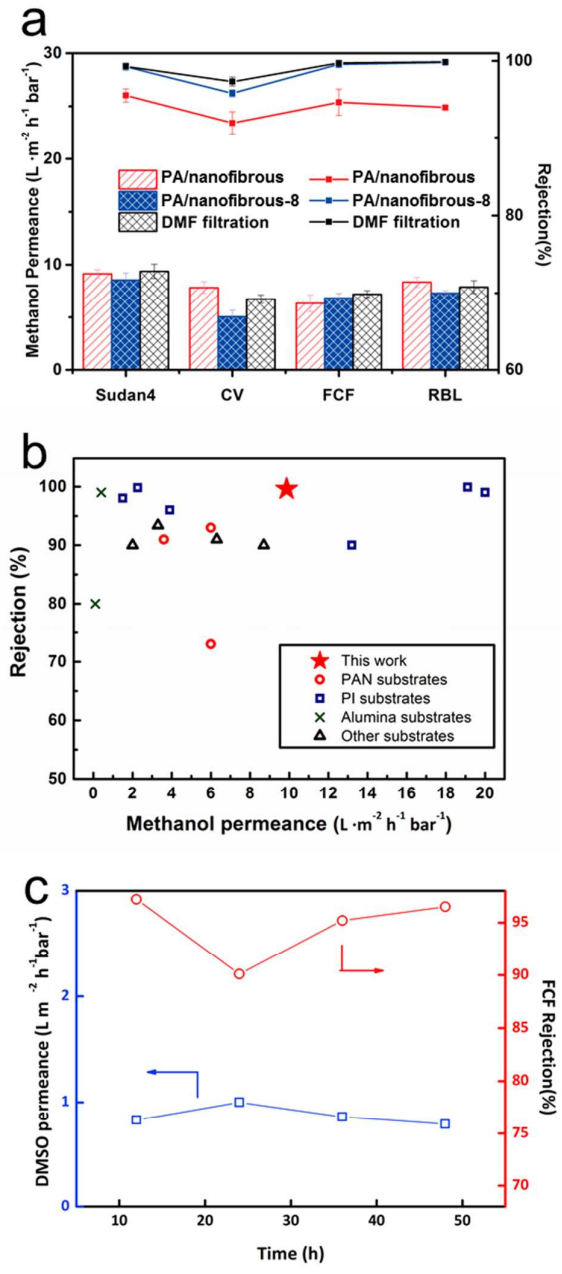


**Fig. 8** (a) Influence of post-treatment in PA/8h-cross-linked nanofibrous substrates performance (b) A comparison of the MeOH permeability and Sudan4 (Mw 380.44 g mol$^{-1}$) dye rejection rates between our membranes and literature. The molecular weight of most dyes reported in these literature ranged between 236 and 535 g mol$^{-1}$ (c) Long-term stability of PA/8h-cross-linked nanofibrous substrates in FCF (808Da)/DMSO system

The methanol flux of TFC membranes with PA selective layers deposited on cross-linked PAN nanofibrous substrates was further enhanced upon DMF activation(**Fig. 8a**). Solvent

activation increase molecular transport through the removal oligomers and resetting the fractional free volume content between polymer chains.[54] The performance of PA/nanofibrous PAN outperformed a range of state-of-the-art membrane [55-68]under comparable conditions (**Fig. 8b & Table S5**). The PA/nanofibrous-8 membrane fabricated in this work out performs previously reported membrane utilizing PAN or other different materials (e.g. PI, PSF, alumina) as substrate, highlighting the importance of a substrate with low tortuosity. It is worthful to note that higher solvent permeance can be achieved when the selective layer were incorporated with nanoparticles, or the membranes were fabricated with ultrathin thickness (sub 10 nm). These may provide useful directions to further improve the performance of thin-film nanocomposite membranes for OSN applications. The PA/nanofibrous PAN membranes were stable in DMSO for up to 50 hours, whilst rejecting more than 95 % of dissolved dyes of different charges and sizes (**Fig. 8c**).

## 4. Conclusion

We demonstrated that electrospinning is an effective fabrication technique to produce polymer substrates with low tortuosity that were crucial for rapid and solvent/solute molecular separations. The high porosity and surface areas of electrospun substrates enhanced uniform cross-linking density that consequently improved solvent stability and mechanical integrity. The newly-developed thin film cross-linked nanofibrous membrane exhibited higher methanol permeance with comparable dye rejections than traditional TFC membranes fabricated from asymmetrical substrates. The thin film cross-linked nanofibrous membrane also demonstrated excellent stability in aprotic solvents such as DMSO; highlighting their potential application in the pharmaceutical industry where active pharmaceutical ingredients are purified from DMSO. The strategy of cross-linking nanofibrous substrates with low tortuosity may provide a paradigm-shifting approach to design next-generation highly permeable and solvent-stable membranes for rapid and stable molecular separations.

## Acknowledgements

The authors gratefully acknowledge the research funding provided by National Natural Science Foundation of China (21506094), Jiangsu Provincial Department of Human Resources and Social Security (JNHB-040), the State Key Laboratory of Materials-Oriented Chemical Engineering (KL17-03). Dr. Shi-Peng Sun is supported by the program of "Thousand Talents Plan-Distinguished Young Professor".

## Notes and references

1. M. S. Chen and M. C. White, *J. Am. Chem. Soc.*, 2004, **126**, 1346-1347.
2. W. X. Zhang, J. Liu and G. Wu, *Carbon*, 2003, **41**, 2805-2812.
3. C. K. Savile, J. M. Janey, E. C. Mundorff, J. C. Moore, S. Tam, W. R. Jarvis, J. C. Colbeck, A. Krebber, F. J. Fleitz, J. Brands, P. N. Devine, G. W. Huisman and G. J. Hughes, *Science*, 2010, **329**, 305.
4. K. H. L., *Ann. NY. Acad. Sci*, 1967, **141**, 131-138.
5. G. Szekely, M. F. Jimenez-Solomon, P. Marchetti, J. F. Kim and A. G. Livingston, *Green. Chem*, 2014, **16**, 4440-4473.
6. Pharmaceutical API/Intermediate Synthesis, http://www.gaylordchemical.com/markets/synthesis/pharmaceutical-api-intermediate-synthesis/, (accessed 21 February, 2018).
7. Z. Wang, S. M. Richter, J. R. Bellettini, Y.-M. Pu and D. R. Hill, *Org.Process.Res.Sci*, 2014, **18**, 1836-1842.
8. M. L. Jue, D. Y. Koh, B. A. McCool and R. P. Lively, *Chem. Mater.*, 2017, **29**, 9863-9876.
9. E. M. Rundquist, C. J. Pink and A. G. Livingston, *Green. Chem*, 2012, **14**, 2197-2205.
10. S. Karan, Z. Jiang and A. G. Livingston, *Science*, 2015, **348**, 1347-1351.
11. J. Zuo and T.-S. Chung, *J. Mater. Chem. A*, 2013, **1**, 9814-9826.
12. J. Zhu, J. Hou, A. Uliana, Y. Zhang, M. Tian and B. Van der Bruggen, *J. Mater. Chem. A*, 2018, **6**, 3773-3792.
13. I. B. Valtcheva, S. C. Kumbharkar, J. F. Kim, Y. Bhole and A. G. Livingston, *J. Membr. Sci*, 2014, **457**, 62-72.
14. K. Vanherck, G. Koeckelberghs and I. F. J. Vankelecom, *Prog. Polym. Sci.*, 2013, **38**, 874-896.
15. D. Chen, X. Liu, D. Li and X. Li, *RSC. Adv*, 2016, **6**, 29570-29575.
16. D. A. Musale and A. Kumar, *Journal of Applied Polymer Science*, 2000, **77**, 1782-1793.
17. X. L. Wu, Y. F. Li, X. L. Cui, J. T. Wang, X. Z. Cao, P. Zhang and L. Y. Zheng, *Acs. Appl. Mater. Inter*, 2018, **10**, 10445-10453.
18. N. Misdan, W. J. Lau, A. F. Ismail and T. Matsuura, *Desalination*, 2013, **329**, 9-18.
19. Z. Tan, S. Chen, X. Peng, L. Zhang and C. Gao, *Science*, 2018, **360**, 518-521.
20. J. M. Yang, C.-S. Fan, N.-C. Wang and Y.-H. Chang, *Electrochimica Acta*, 2018, **266**, 332-340.
21. F. E. Ahmed, B. S. Lalia and R. Hashaikeh, *Desalination*, 2015, **356**, 15-30.
22. Y. K. He, H. Q. Zhang, Y. F. Li, J. T. Wang, L. S. Ma, W. Zhang and J. D. Liu, *J. Mater. Chem. A*, 2015, **3**, 21832-21841.
23. W. E. Teo; and S. Ramakrishna, *Nanotechnology*, 2006, **17**, R89.
24. H. You, X. Li, Y. Yang, B. Wang, Z. Li, X. Wang, M. Zhu and B. S. Hsiao, *Sep. Purif. Technol.*, 2013, **108**, 143-151.
25. S. K. Nataraj, K. S. Yang and T. M. Aminabhavi, *Prog. Polym. Sci.*, 2012, **37**, 487-513.
26. X. Song, Z. Liu and D. D. Sun, *Adv. Func. Mater*, 2011, **23**, 3256-3260.
27. L. Shen, C. Cheng, X. Yu, Y. Yang, X. Wang, M. Zhu and B. S. Hsiao, *J. Mater. Chem. A*, 2016, **4**, 15575-15588.
28. B. S. Lalia, E. Guillen-Burrieza, H. A. Arafat and R. Hashaikeh, *J. Membr. Sci*, 2013, **428**, 104-115.
29. M. Paul and S. D. Jons, *Polymer*, 2016, **103**, 417-456.
30. S. Rajesh, Y. Zhao, H. Fong and T. J. Menkhaus, *J. Mater. Chem. A*, 2017, **5** 4616–4628.
31. S.-F. Pan, Y. Dong, Y.-M. Zheng, L.-B. Zhong and Z.-H. Yuan, *J. Membr. Sci*, 2017, **523**, 205-215.

32. M. S. A. Rahaman, A. F. Ismail and A. Mustafa, *Polym. Degrad. Stab.*, 2007, **92**, 1421-1432.
33. H. G. Hicke, I. Lehmann, G. Malsch, M. Ulbricht and M. Becker, *J. Membr. Sci*, 2002, **198**, 187-196.
34. L. Pérez-Manríquez, J. Aburabi'e, P. Neelakanda and K.-V. Peinemann, *React. Funct. Polym.*, 2015, **86**, 243-247.
35. S. Kaur, R. Barhate, S. Sundarrajan, T. Matsuura and S. Ramakrishna, *Desalination*, 2011, **279**, 201-209.
36. J. Geens, B. V. D. Bruggen and C. Vandecasteele, *Separation & Purification Technology*, 2006, **48**, 255-263.
37. H. M. Tham, K. Y. Wang, D. Hua, S. Japip and T. S. Chung, *J. Membr. Sci*, 2017, **542**, 289-299.
38. F. Li, Y. Dong, W. Kang, B. Cheng and G. Cui, *Appl. Surf. Sci.*, 2017, **404**, 206-215.
39. Z. Han, X. Han, X. Zhao, J. Yu and H. Xu, *J. Hazard. Mater.*, 2016, **320**, 27-35.
40. A. M. Shoushtari, M. Zargaran and M. Abdouss, *Environ. Sci. Technol*, 2010, **101**, 2202-2209.
41. M. S. A. Rahaman, A. F. Ismail and A. Mustafa, *Polym. Degrad. Stabil*, 2007, **92**, 1421-1432.
42. N. Chatterjee, S. Basu, S. K. Palit and M. M. Maiti, *J. Polym. Sci. Pol. Phys.*, 1995, **33**, -.
43. M. Wu, Q. Wang, K. Li, Y. Wu and H. Liuab, *Polym. Degrad. Stabil*, 2012, **97**, 1511-1519.
44. A. M. D. Sayed M. Badawy, *J. Phys. Chem. B*, 2003, **107**, 11273-11279.
45. C. M. Hansen, *Hansen solubility parameters*, Springer New York, 2000.
46. S. Japip, K. S. Liao and T. S. Chung, *Adv. Mater.*, 2017, **29**.
47. S. Japip, K. S. Liao, Y. C. Xiao and T. S. Chung, *J. Membr. Sci*, 2016, **497**, 248-258.
48. S. Oswald and R. Reiche, *Appl. Surf. Sci.*, 2001, **179**, 307-315.
49. A. Greiner and J. H. Wendroff, *Angew. Chem.*, 2007, **46**, 5670-5703.
50. C. H. Lau, B. T. Low, S. Lu and T. S. Chung, *Int. J. Hydrogen. Energ*, 2010, **35**, 8970-8982.
51. P. S. Singh, S. V. Joshi, J. J. Trivedi, C. V. Devmurari, R. A. Prakash and P. K. Ghosh, *J. Membr. Sci*, 2006, **278**, 19-25.
52. S. Sarkar, A. K. Sengupta and P. Prakash, *Environ. Sci. Technol*, 2010, **44**, 1161-1166.
53. G. Hurwitz, G. R. Guillen and E. M. V. Hoek, *J. Membr. Sci*, 2010, **349**, 349-357.
54. A. J. Hill, S. J. Pas, T. J. Bastow, M. I. Burgar, K. Nagai, L. G. Toy and B. D. Freeman, *J. Membr. Sci*, 2004, **243**, 37-44.
55. I.-C. Kim, J. Jegal and K.-H. Lee, *J. Polym. Sci., Part B: Polym. Phys.*, 2002, **40**, 2151-2163.
56. D. Fritsch, P. Merten, K. Heinrich, M. Lazar and M. Priske, *J. Membr. Sci*, 2012, **401**, 222-231.
57. M. F. J. Solomon, Y. Bhole and A. G. Livingston, *J. Membr. Sci*, 2012, **s 423–424**, 371-382.
58. M. Peyravi, A. Rahimpour and M. Jahanshahi, *J. Membr. Sci*, 2012, **s 423–424**, 225-237.
59. M. H. Davood Abadi Farahani and T.-S. Chung, *Chem. Eng. J.*, 2018, **345**, 174-185.
60. M. Navarro, J. Benito, L. Paseta, I. Gascón, J. Coronas and C. Téllez, *ACS Applied Materials & Interfaces*, 2018, **10**, 1278-1287.
61. C. Echaide-Gorriz, M. Navarro, C. Tellez and J. Coronas, *Dalton. T*, 2017, **46**, 6244-6252.
62. S. Karan, Z. Jiang and A. G. Livingston, *Science*, 2015, **348**, 1347.
63. G. Xiangyu, L. Dahuan, H. Tongtong, H. Hongliang, Y. Qingyuan and Z. Chongli, *AlChE J.*, 2017, **63**, 1303-1312.
64. X. Li, C.-A. Fustin, N. Lefevre, J.-F. Gohy, S. D. Feyter, J. D. Baerdemaeker, W. Egger and I. F. J. Vankelecom, *J. Mater. Chem.*, 2010, **20**, 4333-4339.
65. L. Sarango, L. Paseta, M. Navarro, B. Zornoza and J. Coronas, *J. Ind. Eng. Chem*, 2018, **59**, 8-16.
66. N. A. A. Sani, W. J. Lau, N. A. H. M. Nordin and A. F. Ismail, *Chem. Eng. Res. Des.*, 2016, **115**, 66-76.
67. C. Van Goethem, R. Verbeke, S. Hermans, R. Bernstein and I. F. J. Vankelecom, *J. Mater. Chem. A*, 2016, **4**, 16368-16376.
68. X. X. Loha, M. Sairama, A. Bismarcka, J. H. G. Steinkeb, A. G. Livingstona and K. Lia, *J. Membr. Sci*, 2009, **326**, 635-642.

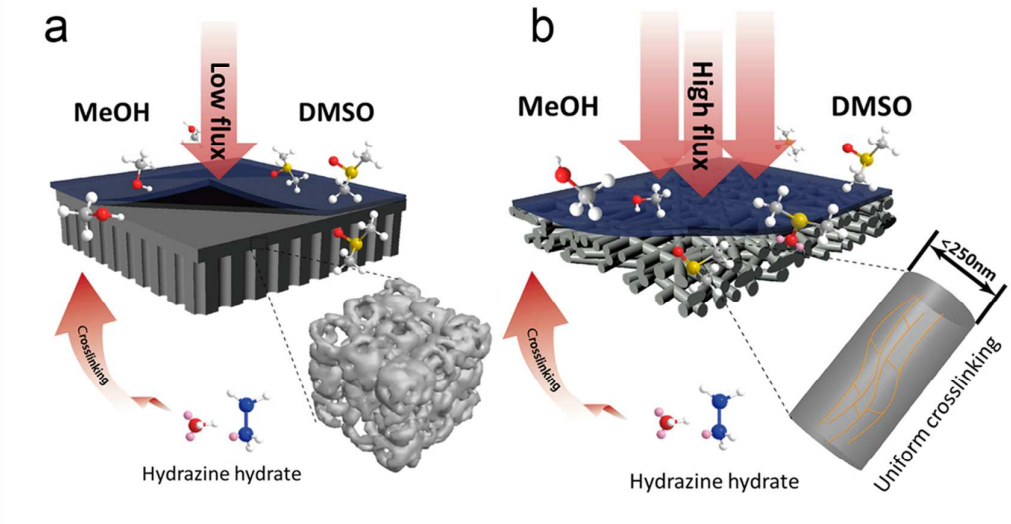


Solvent-resistant thin-film composite nanofibrous membrane : high permeance , high rejection in virtue of high porosity and low tortuosity.